

Quasar Optical Variability in the Palomar-QUEST Survey

Anne Bauer^{1,2}, Charles Baltay¹, Paolo Coppi¹, Nancy Ellman¹, Jonathan Jerke¹, David Rabinowitz¹, Richard Scalzo¹

anne.bauer@aya.yale.edu

ABSTRACT

The ensemble variability properties of nearly 23,000 quasars are studied using the Palomar-QUEST Survey. The survey has covered 15,000 square degrees multiple times over 3.5 years using 7 optical filters, and has been calibrated specifically for variability work. Palomar-QUEST allows for the study of rare objects using multiple epochs of consistently calibrated, homogeneous data, obviating the common problem of generating comparable measurements from disparate datasets. A power law fit to the quasar structure function versus time yields an index of 0.432 ± 0.024 for our best measured sample. We see the commonly reported anticorrelation between average optical variability amplitude and optical luminosity, and measure the logarithmic decrease in variability amplitude to scale as the logarithm of the luminosity times 0.205 ± 0.002 . Black hole mass is positively correlated with variability amplitude over three orders of magnitude in mass. Quasar variability amplitude is seen to decrease with Eddington ratio as a step function with a transition around Eddington ratio of 0.5. The higher variability at low Eddington ratios is due to excess power at timescales shorter than roughly 300 days. X-ray and radio measurements exist for subsets of the quasar sample. We observe an anticorrelation between optical variability amplitude and X-ray luminosity. No significant correlation is seen between average optical variability properties and radio luminosity. The timescales of quasar fluctuations are suggestive of accretion disk instabilities. The relationships seen between variability, Eddington ratio, and radio and X-ray emission are discussed in terms of a possible link between the behavior of quasars and black hole X-ray binaries.

Subject headings: galaxies: active — quasars: general — techniques: photometric

¹Yale University, Department of Physics, P.O. Box 208120, New Haven, CT 06520-8120, USA

²Universitäts-Sternwarte München, Scheinerstr. 1, D-81679 München, Germany

1. Introduction

Quasars are known to be variable in the optical as well as other wavelengths. However, the physics behind the fluctuations is not understood. Flares due to accretion disk instabilities are a promising mechanism (e.g. Pereyra et al. (2006)), but other possible sources of variability include starbursts in the host galaxies (e.g. Aretxaga et al. (1997)) or microlensing of the quasars (e.g. Zackrisson et al. (2003)). Each candidate model can predict variability characteristics such as time dependences and trends with quasar luminosity. Few theoretical results are available with which to compare (e.g. Kawaguchi et al. (1998); Hawkins (2002)), yet qualitative relationships between variability amplitude and quasar properties can elucidate how the fluctuation mechanisms relate to different physical regions and processes in AGN. For example, consider black hole X-ray binaries (BHXBs), which are much less massive systems that also contain central black holes, accretion disks, and sometimes radio jets. Correlations between the variability and other properties such as radio emission and Eddington ratio in BHXBs yield insight into the workings of the system as a whole. The ability to characterize the BHXB behavior into discrete states using these properties is intriguing in terms of the study of quasars.

Recently, as large scale surveys have become feasible, the ensemble optical variability of thousands of quasars has been studied over timescales up to a few years (e.g. Vanden Berk et al. (2004); Rengstorf et al. (2006); Wilhite et al. (2008)) as well as, using archival photographic plates, several decades (De Vries et al. (2005); Sesar et al. (2006)). Most variability work on large quasar samples has been performed by comparing one wide-area dataset with an independent, previous one. This method has yielded many valuable results, but it invariably requires complicated calibrations to correct for the disparate nature of the different measurements. The Palomar-QUEST Survey, by repeatedly covering 15,000 square degrees of sky in optical bands, allows for a robust, consistent analysis of roughly 23,000 spectroscopically confirmed quasars on many timescales over a total span of 3.5 years. We have cleaned and calibrated the survey data for variability purposes and have studied the average quasar variability

amplitude with respect to fluctuation timescale, quasar luminosity, mass, Eddington ratio, X-ray loudness, and radio loudness.

This work uses typically four measurements of each quasar in the sample. Our results describe only the ensemble behavior of the 23,000 objects, as the data are not sufficient to study the detailed variability of each quasar. Individual AGN have diverse lightcurve properties; Collier and Peterson (2001) find a wide range of variability timescales in 12 well-sampled Seyfert 1 galaxies, sometimes measuring several characteristic timescales in a single AGN's lightcurve. In an ensemble study such as our work, using a few measurements of many AGN, such diversity of behavior will be either missed completely or ignored while determining average variability properties. Future work with even larger surveys may be able to bridge the current gap between studies with high quasar statistics and those with detailed lightcurves.

We describe the Palomar-QUEST Survey and its calibrations in §2. The quasar sample is introduced in §3. The structure function, which is the statistical quantity we use to analyze the data, is discussed in §4. Quasar properties, such as mass and luminosity, are often correlated; to study the variability dependence on each separately we divide the data into multi-dimensional bins. This procedure is described in §5. §6 presents our results, which are discussed and compared to previous work in §7. Conclusions are given in §8. Appendix A describes in detail the modelling of the data in order to understand the effects of our observing cadence on the structure function analysis.

2. The Palomar-QUEST Survey

2.1. Overview

The Palomar-QUEST Survey covers roughly 15,000 square degrees multiple times with seven optical filters: Johnson UBRI and SDSS r'i'z'. We use the 48" Samuel Oschin Schmidt Telescope at Palomar Observatory to scan the sky between declinations $\pm 25^\circ$, excluding the galactic plane. The survey is unique in its repeated coverage of such a large area. The time between different scans over the same coordinates ranges from several hours to three years, typically totalling 4 or 5 passes per filter. Often the same sky coordinates were covered

twice in one season, and the whole sky area was observed each year. The wide coverage is made possible by the QUEST large-area CCD camera, which was custom built for the survey. The camera consists of 112 CCDs, each 600×2400 pixels, which are arranged in 4 rows by 28 columns. The survey data were taken in driftscan mode, where the telescope is kept in a fixed position throughout a scan and the stars drift across the field of view of the camera such that every star crosses each of the 4 rows of chips. The stars move parallel to the y coordinates of the chips, and the CCDs are read out in synchrony with the sky motion. The y chip axis therefore is the RA east/west direction, as well as the axis of increasing time throughout the scan. A separate filter covers each row, or finger, so that driftscanning yields nearly simultaneous observations in 4 filters with a fixed exposure time of roughly 140 seconds. The geometry of the camera is shown in figure 1. A typical 8 hour night of observing yields 500 square degrees of data in 4 filters. The camera hardware is discussed in detail in Baltay et al. (2007).

The software used to process the data and yield calibrated object catalogs was written specifically for the survey. The object detection and primary photometry code fit the data to an empirical point spread function (PSF) model, which allows for appropriate deblending of neighboring objects. Photometry is also measured using several apertures. Astrometry is determined through matching with the USNO A-2.0 catalog (Monet et al. (1998)) and is good to $0.1''$. The QUEST processing software is described in further detail in Andrews et al. (2008).

2.2. Variability Calibration

2.2.1. Summary of the Standard Calibration

The standard QUEST photometric calibration consists of two steps: first to correct for the different intrinsic properties of each CCD, and second to compensate for poor weather. The first routine takes into account both the different response levels of the chips, as well as nonlinearities in some chips. The correction coefficients were calculated using a few scans, taken under good conditions, which overlap with the Sloan Digital Sky Survey Data Release 4 (Adelman-McCarthy et al. (2006)) which was used as the reference standard. The sec-

ond step, or extinction correction, uses as a calibration standard for each square degree of sky the QUEST scan over that area for which the objects' measurements are brightest. We use our own data as the calibration standard because there is currently no survey which covers our entire sky area with photometry that is accurate to our precision. Correcting for suboptimal observing conditions is essential to the calibration of the QUEST Survey; we have accumulated so much data because we observe on non-photometric nights. 54% of the extinctions as measured with respect to the extinction correction's reference scans are greater than 0.1 magnitudes. 33% are greater than 0.2 magnitudes. Clearly, to take advantage of the large dataset, we must use an effective extinction correction. Further description of the standard calibration software and performance can be found in Andrews et al. (2008). The calibration is accurate to about 4% in the R, I, r', and i' filters, with roughly 7.5% of the measurements disagreeing with the accepted value by more than 3σ . These outliers appear variable, although the true source of most of them is simply calibration error. In order to use the Palomar-QUEST data for variability purposes, we have developed a new, relative calibration that improves both the average precision of the photometry as well as the percentage of outliers.

The goal of the standard calibration is to produce the most accurate and precise possible average flux measurements of each object. The goal of the relative calibration is for each measurement of an object to be as consistent as possible with each other measurement of the same object. The accuracy of the average flux is less important than the ability to discern intrinsic variability. This shift in priorities between the standard and relative calibrations leads to some differences between the two procedures.

2.2.2. Relative Correction vs. RA or Time

The standard calibration's extinction correction compares overlapping QUEST scans, assumes the one with the brightest measurements of common objects to be photometric, and corrects the other data using that scan as standard. The correction is done using one multiplicative flux constant for each chip for each degree right ascension, which corresponds to about fifteen minutes of data

taken in driftscan mode. This routine is meant to correct for slowly changing weather which causes extinction in the data. However, it is not suited to a relative calibration. It is possible that our scan with the least extinction may in fact be slightly extinguished, moreover in a time-dependent fashion. When we correct other data to this scan we will introduce unwanted time-dependent residuals. The resulting flux measurements will be as close to the photometric values as possible; therefore this procedure is indeed best for the standard calibration. However, the introduced residuals will cause inconsistencies between individual measurements of the objects.

To avoid this situation we select as the “best” scan not the one with the brightest measurements, but the one with the most stable properties throughout the sky area being calibrated. This criterion is quantified using the statistic S given in equation 1. If the QUEST measurements under consideration are consistent with the accepted values, the S distribution will be Gaussian and have unit width. We use the average QUEST magnitudes as the accepted values, and compare them to the magnitudes measured on an individual QUEST scan. If the given scan has changing conditions then the distribution will have greater than unit width. If the given scan has constant data quality then the distribution will be narrow, although it may not be centered on zero. We choose, as the “best” scan for relative calibration purposes, the scan which yields the narrowest such distribution. The scans are ranked separately for each 1/16 square degree of data.

The “best” scan also has the brightest object measurements in only about half of the cases. Much of the discrepancy occurs because different sets of scans are compared in the two cases. The standard extinction corrections are run separately on groups of scans centered near typical QUEST declination pointings, and extinctions are calculated by only comparing data from the same chip on different scans. Because the data are dithered by typically one quarter of a chip width, this organizational scheme includes enough chip overlap to calibrate the vast majority of the QUEST Survey. The extinction calculated for a scan using an overlapping subset of a chip are extrapolated to the remainder of the chip. The relative calibration, however, compares all overlapping data,

including that from neighboring chips or unusual pointings. Furthermore, often a chip will be split between two 1/4 degree declination bins. The relative calibration results are recalculated for each bin rather than extrapolated. Of the “best” scans with non-zero extinction, about 15% have extinctions over 0.1 magnitudes, and 4% over 0.2 magnitudes. These numbers are much smaller than the total data fractions with these extinctions; therefore the relative calibration favors low-extinction data. However, the “best” scans are often indeed extinguished.

The Sloan Digital Sky Survey (SDSS) overlaps roughly one quarter of the QUEST sky area. For these regions, we use SDSS data as the “best” available scan.

$$S = \frac{m_{\text{accepted}} - m_{\text{QUEST}}}{\sqrt{\delta m_{\text{accepted}}^2 + \delta m_{\text{QUEST}}^2}} \quad (1)$$

Using the “best” scan, we apply an RA-dependent, or equivalently a time-dependent, correction to all overlapping scans in the 1/16 square degree under consideration. In each scan, “good quality” objects are chosen with which to determine the calibration, which is subsequently applied to all objects. The “good quality” calibration objects have magnitude greater than 16, so that they are not saturated, and error less than 0.08 magnitudes, so that they have good statistics. The error limit corresponds to a magnitude limit around 19.7 in the R, r', I, and i' filters. Objects with neighbors within 15" are not used for calibration purposes in order to avoid flux contamination from nearby sources. The “best” scan’s calibration objects are matched with those from an overlapping scan, and a line is fit such that

$$m_{\text{best}} - m_{\text{overlap}} = a \times \text{RA} + b. \quad (2)$$

a and b are determined by chi squared minimization, and used to correct the magnitude measurements m from the secondary, overlapping scan. This process is repeated until the “best” scan is used to correct all scans that it overlaps. There may be a scan in the 1/16 square degree that does not overlap the “best” scan; if it does overlap a scan that has been calibrated to the “best” scan, it is calibrated to this intermediate

data. The application of a linear fit rather than a simple constant better approximates changing weather conditions across the sky region.

2.2.3. *Relative Correction vs. Declination*

Variation in chip sensitivity by x coordinate, which corresponds to the declination axis, is accounted for in the first step of the standard calibration. We apply this correction as the first step of the relative calibration as well, since we do want to correct for x -dependent instrumental effects. There exist, however, residual x dependencies since some causes of the sensitivity variations change with time. For example, scattered moonlight yields x -dependent features in the data, and it changes from night to night and also within a single scan. The residual calibration errors in x usually show up as discrete jumps rather than smooth trends; therefore the relative calibration bins the objects by x coordinate and corrects for any discrete jumps observed between objects' magnitudes as measured on an individual scan, and our best estimate of those magnitudes.

Because QUEST images are 600 pixels wide in the x direction and we often dither our central scan declinations by 150 pixels or more, there is typically poor x overlap between different scans. It is therefore impractical to find a single best scan that can be used to correct the rest of the data. After the y dependent correction is applied to each scan, each object's measurements are re-averaged to find an updated mean magnitude. The new mean magnitude is then used as the best value to which to correct. The x dependent calibration is done once for each five degrees RA, or 75 minutes of driftscan, in order to account for slow changes in conditions while accumulating enough statistics to fit a meaningful trend in the x direction. The correction is usually insignificant; only $\sim 2\%$ of measurements are changed by over 0.01 magnitude. However, about 0.5% are corrected by more than their statistical errors, with occasional corrections of several tenths of a magnitude.

2.2.4. *Further Quality Cuts*

More quality cuts are made on the data during the relative calibration than during the standard one, for the purposes of eliminating any remaining calibration tails. These cuts are quite strict;

however they are important to ensuring a reliable variability analysis.

Several cuts are invoked to eliminate spacially extended objects and artifacts from the dataset. The detection and main photometry routines in the QUEST processing software use the data's point spread function (PSF) to deconvolve and measure overlapping objects. PSF routines, however, do not properly measure extended objects, yielding magnitudes that will depend on changing parameters like the seeing. Because the vast majority of quasars appear pointlike in QUEST data, we do not implement further analysis techniques to handle the variability of extended sources. Instead, we use the PSF magnitudes for variability work and simply eliminate objects that appear extended. Because artifacts like unmasked bad columns and saturation trails act like extended objects in the analysis, these are also removed at this stage. Two cuts are implemented for this purpose; their effectiveness was tested using areas of overlap with SDSS.

If a detection appears extended, the PSF routine may deconvolve it into several distinct closeby objects. To eliminate these from the dataset we remove all objects that have a neighbor within $3.5''$. The typical seeing on a good quality night is roughly $2.3''$. This cut throws away a fraction of legitimate stars, but is effective at removing spurious detections that are deblended from a single, extended object and often appear variable. About 11% of all detections are cut at this stage. Roughly 7% of the eliminated objects are stars.

The QUEST photometry routines measure both PSF and aperture fluxes. For pointlike objects, the aperture flux measured in a 1 FWHM radius is typically 15% smaller than the PSF flux. This difference is corrected by separate calibration terms for the PSF and aperture results, yielding consistent measurements for pointlike objects. If an object is extended, the relationship between the PSF and aperture fluxes will change; a comparison of the two fluxes is therefore a test of how well the object conforms to the PSF profile. We eliminate any measurements for which the two measurements differ by greater than 0.1 magnitude. This cut eliminates about 20% of all measurements. However, only roughly 6% of those eliminated are measurements of stars.

Measurements made in regions of the data with

high background noise are also eliminated. Noisy areas often yield poor measurements due to errors in background subtraction, particularly in cases where only small regions of the image have increased sky levels (such as areas close to saturated stars). For each 1/16 square degree of data, the background noise is calculated around each object inside an annulus with inner and outer radii of 30 and 35 pixels from the object’s position. The median of the region’s noise distribution is determined, and the distribution’s natural width is assumed to be reflected by the shape of its lower half. Any asymmetric tail of higher noise will be due to areas with unusually high background, which are likely to yield bad measurements. All objects with

$$\text{noise} > \overline{\text{noise}} + (\overline{\text{noise}} - \text{noise}_{\min}) \quad (3)$$

are discarded, where $\overline{\text{noise}}$ is the median background noise value and noise_{\min} is the smallest measured noise. This eliminates roughly 7% of the data.

Furthermore, for each 1/16 square degree, any scan that contains more than 15% of its measurements outside ± 3 in the distribution of S as defined in equation 1 is disregarded. As before, m_{accepted} is taken to be the average QUEST magnitude measurement of an object and m_{QUEST} is the magnitude measurement from the scan in question. This cut eliminates about 3% of the data, which have serious calibration problems that have not been specifically anticipated by the code.

2.2.5. Evaluation of the Relative Calibration

It is important to have as many measurements of an object as possible if one is to study its variability. In order to accumulate a maximum number of comparable measurements, we have calibrated together data from the Johnson R and SDSS r’ filters, and similarly the Johnson I and SDSS i’ filters. The resulting hybrid bandpasses will be referred to as Rr and Ii. This cross-calibration introduces some error due to uncorrected color terms, but greatly increases the power of the data to study variability by roughly doubling the number of comparable measurements of each object. The color error introduced is larger for the Ii data than for the Rr, since the Johnson R and SDSS r’ filters have very similar wavelength ranges. Because of this effect, the Rr data are used throughout the following analysis rather

than the Ii data. The systematic errors associated with the relative calibration for a random sample of pointlike objects are 0.7% for the Rr data and 1.3% for the Ii data. They are significantly smaller than the $\sim 4\%$ seen in the standard calibration. Figure 2 shows the distribution, for a sample of bright (r magnitude ~ 16) objects, of S after the relative calibration is applied to the data. The relative calibration has very small non-Gaussian tails; now about 2% of the data in a high galactic latitude sample region lie outside ± 3 , rather than 7.5%. Furthermore, as the systematic errors have decreased, the statistic S is sensitive to smaller variations.

To estimate the Rr measurement error for quasars due to uncorrected color terms, we convolved the R and r’ filter transmission curves with various template spectra. The Pickles (1998) template spectra of A through G main sequence stars are used to estimate differences in how the R and r’ filters measure common stars. The calculated broadband R over r flux ratios for these sample objects average 0.986 ± 0.008 , indicating that the two filters treat these stars similarly. In practice, the average offset between the R and r fluxes of typical objects is taken out by the relative calibration. The ratio of R over r calculated flux for the composite quasar spectrum published in Vanden Berk et al. (2001), measured at a range of quasar redshifts between 0.4 and 2.2, is slightly different at 1.023 ± 0.008 . Quasars get bluer when they brighten; Wilhite et al. (2005) measured the changes to be primarily due to the continuum rather than emission lines. They approximated the change in spectral shape between quasars in bright and faint phases as $\Delta F = (\lambda/3060\text{\AA})^{-2.00}$. The R and r’ filter curves yield the same broadband flux for this ΔF spectrum. Therefore we do not expect the quasar color change to increase our color terms, and we estimate the quasar color terms to be roughly 3.5% of the flux, as this is the percent difference between the R to r ratios for main sequence stars and quasars. A 3.5% flux variation corresponds to a structure function amplitude of ~ 0.05 ; fits made in this work include data with average variability starting at roughly twice this level, and usually showing much stronger fluctuations. Therefore the color terms introduced into the quasar measurements by calibrating together R and r data will not strongly

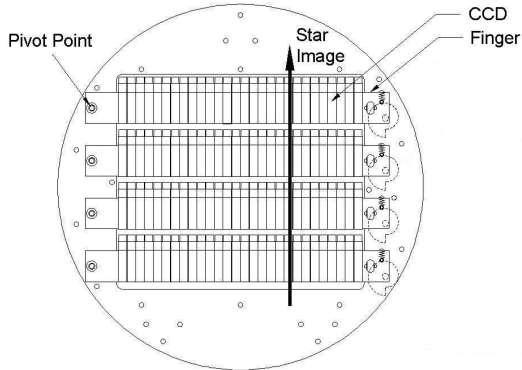


Fig. 1.— The QUEST camera design, showing the 112 CCDs arranged on 4 rows, or fingers.

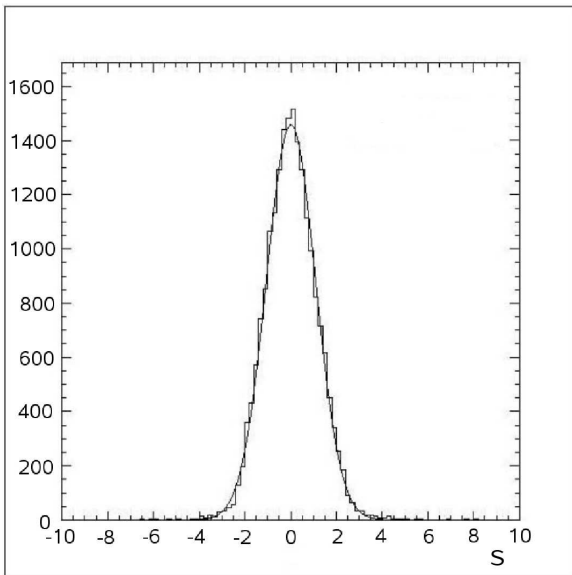


Fig. 2.— Distribution of S , as defined in equation 1, after relative calibration. A Gaussian fit is superimposed.

affect our results.

We can quantitatively compare the variability that we see with that measured by other surveys. Huber et al. (2006), as part of the Faint Sky Variability Survey (FSVS), studied ~ 3.5 degrees² observed 12 – 15 times over timespans from hours to 3 years and determined what fraction of observed objects appeared variable, for various object magnitude bins and variability amplitudes. The relatively small areal coverage of their study means that the statistics are low for rare, highly variable objects; however they see that roughly 0.5% to 1% of all objects between magnitudes 17.5 and 18.5 have variability amplitudes of at least 0.1 magnitude in the V band. We see that 0.6% of objects with Rr magnitudes between 17.5 and 18.5 vary with amplitudes greater than 0.1 magnitude simultaneously in the Rr and Ii bands. To determine this statistic we require a 0.1 magnitude jump to be significant to 3σ in both the Rr and Ii bands. This requirement is not satisfied by most objects fainter than magnitude Rr ~ 18.5 ; therefore we limit the comparison to objects brighter than this value. In this range of magnitude and variability amplitude overlap between Palomar-QUEST and the FSVS, our observations agree very well.

3. The Quasar Sample

We have studied the variability of a sample of SDSS spectroscopically identified quasars. SDSS covers a substantial fraction (roughly one quarter) of the QUEST area, and has to date measured over 100,000 quasars. Spectroscopic identification ensures that the sample is close to 100% pure, and the spectra provide supplemental information such as line widths that allow us to estimate parameters like the mass of the quasar’s black hole. Furthermore, accurate knowledge of the quasar redshifts is crucial for studying the rest-frame time dependence of variability.

25,043 SDSS spectroscopic quasars, published as of April 2007, lie in the QUEST sky area. On average we have slightly more than four good quality, relatively calibrated measurements of each quasar in the Rr band. For a few objects we have over twenty; a histogram of the number of QUEST Rr measurements of each quasar is shown in figure 3.

Because some blazars (e.g. FSRQs) have

quasar-like optical spectra, there may be blazars contaminating this spectroscopically identified quasar sample. Blazar flux is dominated by beamed jet emission while quasar flux is thought to be primarily from the accretion disk; before examining the objects in order to study the causes of quasar variability it is important to eliminate any known blazars from the list. Cross-checking with several blazar catalogs (Stickel et al. (1991), Giommi et al. (2002), Healey et al. (2007), Sowards-Emmerd et al. (2005), Hewitt et al. (1993), Massaro et al. (2007), Turriziani et al. (2007), Collinge et al. (2005), and Veron-Cetty and Veron (2006)) reveals 47 blazars in the sample. Furthermore, there are 92 objects that show dramatic variability in the QUEST Survey that is uncharacteristic of typical quasar behavior. They are seen to vary by more than 0.4 magnitudes over the course of the ~ 3.5 years of our survey, which matches better with the behavior of known blazars than with quasars. (The typical variability of blazars in the QUEST Survey will be studied in a future paper.) Two of the 92 variables are among the 47 known blazars; therefore we remove in all 137 objects from the list.

As mentioned earlier, extended objects will not be measured properly by the PSF photometry routines. A conservative method of removing objects which are not pointlike in our data is to eliminate those that are found to be extended by SDSS. SDSS goes roughly one magnitude deeper than QUEST in the r' filter and has seeing of $1.4''$ as opposed to our $2.3''$. The quasars in their photometric database are largely marked as morphologically pointlike past a redshift of 0.4, but mostly extended closer than that. We therefore do not study those objects that have redshifts less than 0.4 so that we can be confident that the extent of the objects does not introduce significant systematic measurement errors. After this cut we are left with 22,825 quasars in our final sample.

Radio and X-ray information is known for small subsets of these quasars. We gather radio fluxes by matching the quasars with the FIRST Survey (Becker et al. (1995)). A matching radius of $5''$ yields 1,986 quasars with measured 1.4 GHz radio fluxes. X-ray luminosities at 2 keV are taken from Anderson et al. (2007), which carefully cross-matches SDSS quasars from their data release 5 with the ROSAT All-Sky Survey. 847 of the

quasars in our sample have such X-ray measurements.

4. The Structure Function

There are many ways to parameterize variability. The structure function (SF) has been used by a number of studies to examine quasar variability (e.g. Vanden Berk et al. (2004), De Vries et al. (2005)). It is defined in several ways in the literature. Two common definitions are as follows:

$$SF^{(A)}(\tau) = \sqrt{\langle [m(t) - m(t - \tau)]^2 \rangle - \langle \sigma^2 \rangle} \quad (4)$$

$$SF^{(B)}(\tau) = \sqrt{\frac{\pi}{2} \langle |m(t) - m(t - \tau)| \rangle^2 - \langle \sigma^2 \rangle} \quad (5)$$

$m(t) - m(t - \tau)$ is the difference in measured magnitudes of an object at two different times, where the times are separated by an interval τ in the quasar rest frame. σ is the measurement error on the magnitude difference term so that the structure function measures only the intrinsic variations in the quasar flux. $\langle X \rangle$ denotes the mean value of X measured for the set of objects. The form given in equation 5 was introduced by Di Clemente et al. (1996) because it is more robust to outliers than that given in equation 4. The two forms are equivalent if $[m(t) - m(t - \tau)]$ comes from a Gaussian distribution. If this is true, then outliers in the data will tend to be measurement errors and equation 5 will accurately reflect the physics. If the underlying variability distribution is not Gaussian, however, these two equations are not equivalent and equation 4 describes the variability statistics in the most straightforward way, as it is directly related to other statistical quantities such as the autocorrelation function and the variance. Because other studies have published results using variously $SF^{(A)}$ or $SF^{(B)}$, we have analyzed the QUEST data using both forms in order to compare with all of the available literature.

A plot of the structure function vs. time lag has a characteristic shape based on the variability properties of the data. For short timescales, where the intrinsic variability amplitude is smaller than the noise, the structure function will be flat with amplitude $\sqrt{2}\sigma^2$. For timescales shorter than those characteristic of the variability, but where

variability can be measured, the structure function rises proportional to τ . At timescales typical of the variability the structure function has a shape that depends on the details of the system’s lightcurves. For timescales longer than those of the variability, the structure function is again flat, with amplitude $\sqrt{2\sigma_{sys}^2}$ where σ_{sys} is the average magnitude variation of the system. These features would be evident in structure functions calculated from evenly sampled datasets over timescales much longer than those of the system’s variability, in which edge effects and aliasing are negligible. In finite, clumpy datasets such as ours the shape of the structure function may be affected by the data cadence, also called windowing. This dependence is explored in appendix A; in summary, windowing does not significantly alter the slope of the rising portion of the structure function, although it can introduce an artificial turnover at long time lags.

5. Managing Correlated Quantities

Quasar optical variability has been seen to depend on parameters other than timescale. For example, the variability amplitude is well-known to be anticorrelated with optical luminosity (e.g. Helfand et al. (2001); Vanden Berk et al. (2004)). It has also been seen that variability amplitude increases with quasar black hole mass (Wold et al. (2007); Wilhite et al. (2008)). Some correlations between quasar properties may simply be artifacts of the data, such as relationships between luminosity and redshift for objects discovered in flux-limited surveys. In order to understand which intrinsic characteristics of the quasars most strongly influence the variability, we must treat the objects’ parameters as independently as possible. We accomplish this using a method described below, which is similar to that used in Vanden Berk et al. (2004)

There are four basic quantities that we know for all of the quasars in our sample: rest frame time lag τ between measurements, optical luminosity L , estimated black hole mass M_{BH} , and redshift z . There are known correlations between all of these parameters, either due to physical relationships or due to the biases of flux limited surveys, or perhaps a combination of both. To avoid these complications and look at the dependence of variability on only black hole mass, for example,

we would like to take a set of quasars with identical properties except for their black hole mass, and then examine how the variability differs between them. To approximate this procedure, we have split each parameter’s range into bins: six bins each in time lag, luminosity, mass, and redshift. The choice of bin limits is shown in table 1. Quasars with values outside the given ranges are not included in the analysis. 25% of the quasar measurements are excluded due to the L , M_{BH} , and z limits. A further 35% fall outside the τ bin limits, which are chosen to exclude data affected by systematics at low τ and windowing at high τ . The motivation for the exact τ limits are discussed in section 6.2.

In each multi-dimensional bin we calculate the average variability amplitude of the objects using the equation

$$V = \sqrt{\langle (\Delta m)^2 \rangle - \langle \sigma^2 \rangle} \quad (6)$$

which is identical to the structure function form $SF^{(A)}$ except it is not a function of τ but instead compares all available measurements of the same quasar. Then, holding constant the bin indices for time lag, luminosity, and redshift, we can legitimately compare the six bins of black hole mass. This procedure yields $6 \times 6 \times 6 = 216$ possible six-point plots of variability amplitude V vs. mass, or 1296 possible V values. Most of the combinations of parameters do not describe many objects in our sample. In order to determine a statistically significant value of V , we require 100 measurement pairs in a bin before including it in the analysis. The number of measured V s is therefore

	τ	z	M_{BH}	L
Min	100	0.4	10^7	29
Bin Divisions	150	0.7	5×10^8	29.75
	210	1.0	10^9	30.25
	280	1.3	2×10^9	30.75
	350	1.6	3×10^9	31.15
	425	1.9	5×10^9	31.55
Max	500	2.2	8×10^9	32

Table 1: Quasar sample bin limits introduced to handle correlated quantities orthogonally. Units of τ : days; M_{BH} : $\times M_{\odot}$; L : $\text{Log}(\frac{\text{erg}}{\text{s}\cdot\text{Hz}})$ measured at 2500 Å.

much smaller than 1296 due to statistics. In fact, we measure 148 well-sampled V values. To examine the overall behavior of the variability amplitude in terms of the mass we can normalize the six-point measured trends together and average the resulting normalized data in each mass bin in order to find a simple, meaningful result of how the variability scales with the quasar’s mass (or any of the other parameters). Because the data are arbitrarily normalized to the set with the best statistics, the exact values for V should not be taken seriously. The shape of the trend is the important result. The normalization process is illustrated in figure 4. Panel (a) shows two unnormalized datasets of $\log(V)$ versus an example parameter. For simplicity, each point is assumed to have equal uncertainties, which are not shown. The $+$ dataset will be normalized to the \times dataset, as the \times dataset has the higher statistics. The normalization consists of an additive constant on the log scale, in order to preserve the power law shapes observed in the V vs. time and luminosity trends. The constant is determined by minimizing the chi squared difference between the values from the two datasets in the same bin, for the bins where there exist data from both sets. Panel (b) in figure 4 shows the data after the $+$ data are shifted by one constant such that they best agree with the \times data. Panel (c) shows the final result after averaging the normalized data in each bin.

6. Results

6.1. Variability vs. Optical Luminosity

$\log(V)$ vs. $\log(L)$ for the quasar sample, where L is the luminosity of the quasar calculated at a rest frame wavelength of 2500 \AA , is shown in figure 5. 2500 \AA is chosen because it is a wavelength dominated by continuum emission that, for the redshift range of the sample, lies predominantly in the high-throughput SDSS g , r , or i filters. The luminosity at rest frame 2500 \AA is determined by convolving a redshifted composite quasar spectrum taken from Vanden Berk et al. (2001) with the SDSS filter curves and using the SDSS broadband flux measurements to normalize the composite spectrum’s amplitude. The flux at any particular wavelength is then given by the normalized composite spectrum, and can be converted to luminosity using the object’s redshift

and the cosmological parameters which we assume to be $\Omega = 1, \Omega_\Lambda = 0.7, \Omega_M = 0.3, H_0 = 71 \frac{\text{km}}{\text{s}\cdot\text{Mpc}}$. The downturn in figure 5 at low luminosities is most likely an artifact of our magnitude limit; if a faint quasar becomes dimmer we may not see it. We will then not observe the whole range of variability for the faintest objects. There are relatively few statistics in the first two luminosity bins, contributing to a large systematic error as well: the first bins contain 4 and 10 measurements, respectively, compared to between 31 and 63 in the remaining bins. We fit a line to the four brightest points in figure 5 and find a slope of 0.205 ± 0.002 . The reduced χ^2 of the fit is very small: $\chi^2 = 0.1735$.

The errors on the points in this and all subsequent plots are the 1σ standard deviation of values obtained by analyzing subsets of the total sample.

The observed trend of average variability amplitude with luminosity implies that we do not fully measure the variability of low-luminosity objects. For this reason, quasars with luminosity less than $10^{30.5} \frac{\text{erg}}{\text{s}\cdot\text{Hz}}$ are not included in the remaining analysis unless stated otherwise.

6.2. Quasar Structure Function vs. Time

In order to show results comparable to other published work we have calculated the structure function, binning only in rest frame time lag and not in other parameters such as luminosity, using both forms $SF^{(A)}$ and $SF^{(B)}$. This analysis does include quasars of all luminosities. The results are shown as solid points in figure 6, along with, as \times s, analogous results for a random sample of pointlike objects. The quasar structure function rises approximately as a power law. The turnover we see at long time lags is due not to intrinsic qualities of the variability, but to windowing effects as described in appendix A. The power law index, often called the structure function slope since the data tend to be plotted on a log-log scale, is measured to be 0.357 ± 0.014 using $SF^{(A)}$, and 0.3607 ± 0.0075 using $SF^{(B)}$. The two results agree with each other to within 1σ ; we adopt the form $SF^{(A)}$ for use in the rest of the structure function analyses.

In the case of $SF^{(A)}$ we iteratively clip the data to reduce the effects of measurement errors and atypical objects. To ensure that the struc-

ture function slope is not sensitive to the details of the clipping, we only fit the points in $SF^{(A)}$ whose clipping quickly converges. The time lag bins with low variability amplitude are most affected by outliers; therefore only longer time lag bins, with $\tau > 100$ days, are included in the fit. The presence of low- τ outliers may partially be due to color terms in the data, which contribute at a level of $SF \sim 0.05$. The last several structure function points suffer from edge effects due to the QUEST data cadence, as examined in appendix A. So, $SF^{(A)}$ is fit between rest frame time lags of 100 and 500 days; these limits are also used in the binned $V(\tau)$ analysis described in section 5. The $SF^{(B)}$ fit includes data at smaller time lags since this form is designed to minimize the effects of outliers in the data. For the $SF^{(B)}$ result, then, we fit all time lags shorter than 600 days, after which the windowing effects become prominent.

The structure functions of a random sample of pointlike objects, also shown in figure 6, are flat. The errors on these data vary substantially from point to point because the objects are assumed to be stars at zero redshift, so there are low statistics at multiples of half-year rest frame time lags.

We have also calculated the quasar structure function vs. rest frame time lag using the multi-dimensional binning and normalizing technique described in section 5. This procedure, when performed using quasars of all luminosities, yields a structure function slope of 0.392 ± 0.022 , which agrees with our other measurements to within the 1σ for the $SF^{(A)}$ result and 1.1σ for the $SF^{(B)}$ result. We expect this similarity because the correlation between the rest frame time lag between observations of a quasar and the quasar’s redshift is most pronounced at the extremes of the time lag distribution and we are only fitting a middle range. Furthermore, there is no reason why the time lag between our observations of certain quasars would depend on intrinsic properties like their mass or luminosity. Therefore we expect the fit to be minimally affected by the binning. When restricting the analysis to only those quasars with luminosity at rest frame 2500 Å greater than $10^{30.5} \frac{\text{erg}}{\text{s}\cdot\text{Hz}}$, as motivated in section 6.1, the measured slope increases to 0.432 ± 0.024 . This latter result is a better measurement of the quasars’ variability behavior with time lag, as it excludes objects whose faintest states appear to be below our flux limits.

6.2.1. Lightcurve Asymmetry

The shape of quasar flares holds information about the flares’ physical source. Because there are typically only four QUEST measurements of each quasar, we can not study the detailed lightcurve shapes of the 23,000 quasars individually. However, we can examine any flare asymmetry by calculating the structure functions from brightening and fading subsets of the data, i.e. the measurement pairs for which $m(t) > m(t + \tau)$ and $m(t) < m(t + \tau)$, respectively. If the variability were due to flares which brightened over a month and faded over a year, a structure function calculated using only brightening magnitude pairs would have more power on a month timescale and less on a year timescale than one calculated using only fading magnitude pairs. Figure 7 shows the brightening and fading structure functions, calculated without multi-dimensional binning, for all quasar luminosities, using $SF^{(A)}$. The asterisks illustrate the brightening measurements and the solid points reflect the fading ones. There is no evidence for any flare asymmetries over the timescales that we measure; the two structure functions are consistent with each other to within errors.

6.3. Variability vs. Black Hole Mass

Given a quasar spectrum, one can estimate the black hole mass. The method we use is based on that of Kaspi et al. (2000), further discussed in e.g. Shields et al. (2003) and Salviander et al. (2007), and thought to be good to a factor of 3. Given that our quasar sample spans two orders of magnitude in mass, the error associated with this calculation will not mask a global trend. We calculate each quasar’s black hole mass using the equation

$$\begin{aligned}
 M &= (10^{7.69} M_{\odot}) \\
 &\times \frac{[\sigma_{\text{H}\beta}, \sigma_{\text{MgII}}]}{3000 \text{ kms}^{-1}} \\
 &\times \sqrt{\frac{\lambda L_{\lambda 5100}}{(1044 \text{ ergs}^{-1})}}.
 \end{aligned}
 \tag{7}$$

where $[\sigma_{\text{H}\beta}, \sigma_{\text{MgII}}]$ is the full width at half maximum of the $\text{H}\beta$ or MgII emission line, depending on which is available in the SDSS database.

If both are measured, we use the average of the two values. $L_{\lambda 5100}$, the luminosity of a quasar at 5100 Å, is calculated from the SDSS broadband fluxes in the same manner as $L_{\lambda 2500}$, as described in section 6.1. The logarithm of the quasar variability amplitude V vs. the logarithm of the estimated black hole mass, calculated after multi-dimensional binning, normalization, and averaging, is shown in figure 8. We see a significant increase in quasar variability amplitude with black hole mass over the entire mass range studied. However, it is a much smaller effect than that seen with respect to time lag or luminosity.

It is important to note that the relationship between variability amplitude and luminosity entirely masks the trend with black hole mass if the results are calculated without regard to the correlation between the quasars' properties. The brightest quasars are usually the most massive, which leads to the apparent result that the massive quasars vary least. Once the luminosity effects are separated out, however, the trend completely reverses to show an increase in variability amplitude with mass.

Because physical timescales such as the accretion, dynamical, and thermal timescales of AGN disks scale with black hole mass, it is plausible that optical variability timescales might differ between AGN of different masses. However, the average variability amplitude V versus time, calculated separately using low, medium, and high mass subsets of the data, yield consistent results.

6.4. Variability vs. Eddington Ratio

The Eddington ratio is the object's bolometric luminosity L_{bol} divided by its Eddington luminosity L_{edd} , and is a useful parameter describing the accretion rate of the central engine. It can be estimated using the equation

$$E \equiv \frac{L_{\text{bol}}}{L_{\text{edd}}} \approx \frac{9 \times \lambda L_{\lambda 5100}}{1.3 \times 10^{38} (M_{\text{BH}}/M_{\odot})} \quad (8)$$

where the approximation for the bolometric luminosity is that made by Kaspi et al. (2000).

Because the black hole mass estimate, M_{BH} , is uncertain to roughly a factor of three, the Eddington ratio is as well. M_{BH} is thought to be an overestimate as often as an underestimate, so the

net effect on the results is a smearing of the values rather than a systematic shift. The consequence of any error in M_{BH} will therefore simply cause a flattening of the results rather than introduce a spurious trend.

To calculate the dependence of variability amplitude on Eddington ratio we reorganize the data, substituting both the black hole mass and luminosity binning for one binning in Eddington ratio. The dependencies on time lag and redshift continue to be normalized out as before.

The resulting plot of $\text{Log}(V)$ versus Eddington ratio is shown in figure 9. The average variability amplitude decreases with increasing ratio. The calculated Eddington ratios of the quasars are predominantly between zero and one, but include a very long, small tail out to large values, which may be due to poor luminosity or black hole mass measurements. The point shown at 1.1 on the x axis is in fact calculated using all quasars with estimated Eddington ratios between one and ten.

To examine the timescales on which the quasars with different Eddington ratios vary, we have calculated the structure function versus time for only objects with low Eddington ratios between 0 and 0.4, and again for only objects with high Eddington ratios between 0.6 and 1. The results are shown in figure 10, where the solid circles show the data with low Eddington ratios and the \times symbols indicate data with high Eddington ratios. At time lags shorter than roughly 300 days, the low Eddington ratio quasars are consistently more variable than those with high ratios. The trend is reversed at longer time lags.

6.5. Variability vs. X-ray Emission

Because we have X-ray information for only a small subset of the quasars, we split the X-ray values into only three bins: bin 0 includes all objects with no X-ray information, bin 1 holds objects with X-ray slope α_{ox} greater than 1.35, and bin 2 holds those with α_{ox} less than 1.35. α_{ox} is defined as the exponent of a hypothetical power law interpolated between the 2 keV X-ray and the 2500 Å optical measurements of the object, as is used in works such as Anderson et al. (2007). Bin 2 is X-ray louder than bin 1, with the division chosen so that the two bins have roughly equal numbers of objects. It is important to note that

since we are normalizing out the effects of optical luminosity, our X-ray results are closer to a variability trend with X-ray luminosity rather than with X-ray loudness.

Splitting the X-ray detected quasars into subsets by α_{ox} , time lag, redshift, luminosity, and black hole mass leaves very few objects in each bin. To gain enough statistics to calculate V , we collapse the time lag and redshift bins and only divide the quasars by α_{ox} , luminosity and mass. Furthermore, we insist on only 50 measurement pairs (rather than 100) as a minimum for calculating V . If the X-ray loudness is correlated with redshift (or, improbably, with time lag between QUEST observations) then the relation we measure between variability and α_{ox} will be confused with any relation between variability and redshift or time lag. The redshift distributions of the X-ray louder and X-ray quieter quasars are quite similar, however, so any variability trends with redshift will contribute similarly to each bin. The correlations between X-ray loudness and optical luminosity and mass are indeed normalized out of the results, which are given in table 2.

These results show a 2.9σ anticorrelation between optical variability amplitude and X-ray emission. The quasars for which we have no X-ray information have an average optical variability amplitude intermediate between the values for the X-ray fainter and X-ray brighter samples.

6.6. Variability vs. Radio Emission

As is the case with the X-ray data, only a small subset of the quasars has radio measurements. To calculate V with the available statistics we make the same concessions as in the X-ray analysis: computing V with a minimum of 50 measurement pairs and eliminating the time lag and redshift binning. Any correlation between redshift and radio

X-ray Emission	Log(V)
Unknown	-0.941 ± 0.006
Fainter Subset	-0.813 ± 0.024
Brighter Subset	-1.022 ± 0.049

Table 2: Variability Log(V) for quasars of different X-ray emission. Bins correspond roughly to X-ray luminosity, as described in the text.

loudness will not be removed; therefore if the redshift and radio properties are correlated then the variability dependence on these parameters will be confused. However, the redshift distribution of the radio subsamples are similar, implying no strong relationship between radio loudness and redshift for our sample. The quasars are divided into three radio bins: bin 0 includes all objects with no radio information, bin 1 has objects with ratios R of 5 GHz radio to 4500 Å optical luminosity below 20, and bin 2 has objects with R above 20. The definition of radio loudness R follows that of authors such as Peterson (1997), and the break point between the two radio subsets was chosen so that each bin has roughly equal numbers of objects. As with the X-ray sample, it should be noted that once the normalization is performed, the measurements are divided according to a measure closer to luminosity than to loudness.

The logarithm of the quasar variability amplitude V for samples with different radio emission is given in table 3. The three measurements agree within their errors; we therefore see no evidence for a change in the average optical variability amplitude with increasing radio luminosity.

The observed trend of decreasing variability amplitude with increasing optical luminosity has previously been seen only in radio quiet quasars, prompting Helfand et al. (2001) to hypothesize different variability mechanisms for radio loud and quiet objects. To see if the luminosity trend that we observe is the same for radio louder and quieter quasars in our sample we examine the log(V) vs. optical luminosity using only objects in one radio bin at a time. The results are shown in figure 11: the first panel includes radio quieter quasars (those with $R < 20$); the second panel includes radio louder ones (with $R > 20$). We see that the trend indeed exists in both samples, even appearing stronger in the radio loud objects.

Radio Emission	Log(V)
Unknown	-0.870 ± 0.005
Fainter Subset	-0.880 ± 0.027
Brighter Subset	-0.880 ± 0.028

Table 3: Variability Log(V) for quasars with different radio emission. Bins correspond roughly to radio luminosity, as described in the text.

7. Discussion

7.1. Structure Function vs. Time Lag

The slope of the structure function versus rest frame time lag has been measured for several large ensembles of quasars, using different types of data, different time scales, and different definitions of the structure function. It is therefore not straightforward to compare all of the results.

We have calculated the structure function slope in four ways: first, using equation 4 and binning the data only in time lag; second, using equation 5 and binning the data only in time lag; third, using equation 4 and normalizing the data after binning it in luminosity, mass, and redshift; and fourth, identical to the third method but only including quasars with 2500 Å luminosity greater than $10^{30.5} \frac{\text{erg}}{\text{s}\cdot\text{Hz}}$, at which level we are confident we can measure the full range of typical variability. The last result is the most robust measurement, but if faint quasars have different variability timescales than bright ones then we are only observing one end of the behavior.

Our results are compared to others from the literature in table 4. Because our results using structure functions defined by equations 4 and 5 are consistent with each other, we do not distinguish in the table between results using the different forms. In table 4, QUEST2 refers to this work. QUEST1 refers to Rengstorf et al. (2006), who studied 933 quasars using the QUEST I Variability Survey. Each quasar had roughly 25 measurements in the Johnson R band, and the structure function slope was fit between 50 and 600 days. SDSS + Plates refers to work by De Vries et al. (2005), in which SDSS data were compared with POSS and GSC2 archival data in order to generate a dataset that spanned roughly 50 years. The structure function slope was fit over timescales of one to twenty years, over which the data appears to follow a power law. After these timescales their structure function appears to flatten, although the authors note that the longest timescale data is noisy and does not indicate a significant plateau in the structure function. However, Sesar et al. (2006) also studied SDSS and POSS data that spanned several decades and saw that the variability amplitude on decade timescales is smaller than that expected from an extrapolation of power law results fit using ~ 3 years of data. SDSS + Spectra

in table 4 refers to Vanden Berk et al. (2004), who compared SDSS broadband measurements to spectrophotometry calculated from the SDSS spectra which identified the objects as quasars. They calculated the structure function slope before and after binning and normalizing their data in a manner similar to our method. SDSS Equ. denotes the Wilhite et al. (2008) study of quasars with ~ 10 SDSS measurements in a 278 square degree equatorial region. The study focuses mainly on the links between variability and mass, luminosity, and therefore Eddington ratio. To compare with other variability work they measure $SF^{(B)}$ of the sample, although they do not provide an error estimate.

A different kind of AGN variability study was done by Collier and Peterson (2001). Their sample consists of 12 Seyfert 1 galaxies with masses $\sim 10^7 M_{\odot}$, observed every few days for up to several years. The average structure function slope, measured over timescales of about 5 to 60 days, is listed as Sy1 in table 4. Because they have many observations of the AGN they calculate the structure functions of each separately and see clear characteristic timescales of variability for each object. The timescales differ widely between the AGN, ranging from 5 to 100 days. The average structure function slope of these Seyferts disagrees with our best value by 2.3σ . However, the Seyferts' structure functions differ significantly from each other; six out of the twelve structure function slopes are consistent with ours. Although we see no evidence for a turnover in the Palomar-QUEST ensemble structure function, it is likely that the individual objects in our sample may show structure function plateaus at various timescales. Such a detailed study of individual quasars requires more data than is available from the Palomar-QUEST Survey.

Table 4 compares these different published results to the most comparable measurements from this work. The QUEST1, SDSS + Plates, one of the SDSS + Spectra, and the SDSS Equatorial results do not take into account correlations between variability and other parameters such as luminosity or redshift; these are compared to our unnormalized measurement. One SDSS + Spectra measurement does deal with the parameter interdependencies; this is compared to our normalized result. Our most robust result conservatively cuts

out lower luminosity quasars; there is no directly comparable result in the literature, but we include the measurement in the table as it is the most reliable.

Kawaguchi et al. (1998) and Hawkins (2002) present theoretical structure function slopes calculated from example disk instability, starburst, and microlensing models. These slope predictions are shown in table 5. Our and most of the other results in table 4 agree best with the disk instability prediction, although the models explored by those papers are by no means definitive; more theoretical results with which to compare are needed.

We see no evidence for asymmetry in quasar lightcurves over the timescales measured, as shown in figure 7. De Vries et al. (2005) calculated brightening and fading quasar structure functions over long timescales using several datasets and saw significant asymmetry on timescales of 2 to 3 years. They suspect the asymmetry to be stronger than measured due to the dampening effects on the measurement by Malmquist bias. Because our epochs are taken from the same dataset and the measurements at all epochs are treated identically, Malmquist bias will not affect the QUEST results. The timescales on which asymmetry was observed by De Vries et al. (2005) lie in our longest timescale bins, which have large statistical and systematic errors. Our null result is therefore not inconsistent with their asymmetry detection.

7.2. Variability vs. Optical Luminosity

The well-known trend that optically luminous quasars have fractional variability that is, on average, smaller than that of faint quasars is qualitatively consistent with the hypothesis that the variability is due to the cumulative effects of small discrete flares. The details of the relationship between variability amplitude and quasar luminosity depend on the source of the variability. For example, if the fluctuations were due to a Poissonian distribution of flares, each with identical timescale and energy, the following relationship would hold (Cid Fernandex et al. (2000)):

$$\frac{\Delta L}{L} \propto \bar{L}^{-\delta} \quad (9)$$

where $\delta = \frac{1}{2}$. This scenario is clearly too simplified to reflect the properties of quasar variability;

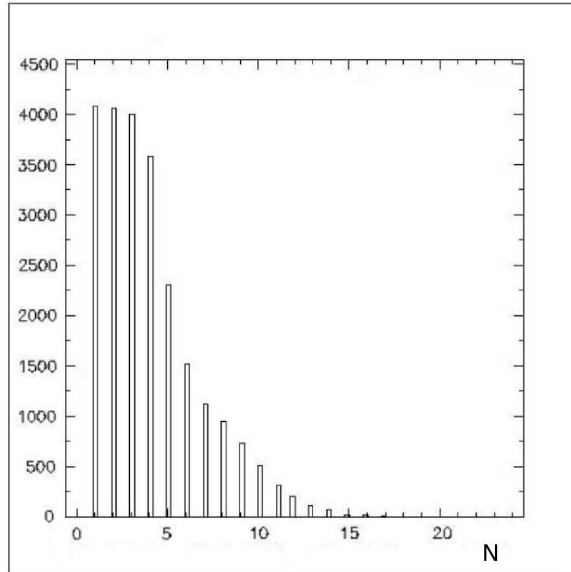


Fig. 3.— Number of quasars with N good Rr measurements, versus N .

Experiment	SF Slope	Ref.
Unnormalized		
QUEST2	0.357 ± 0.014	(1)
QUEST1	0.47 ± 0.07	(2)
SDSS + Plates	0.30 ± 0.01	(3)
SDSS + Spectra	0.336 ± 0.033	(4)
SDSS Equ.	0.486	(5)
Sy1	0.555 ± 0.030	(6)
Normalized		
QUEST2	0.392 ± 0.022	(1)
SDSS + Spectra	0.246 ± 0.008	(4)
Normalized, Bright		
QUEST2	0.432 ± 0.024	(1)

Table 4: Comparison of experimental quasar structure function slopes. Reference (1) indicates this work. (2): Rengstorf et al. (2006). (3): De Vries et al. (2005). (4): Vanden Berk et al. (2004). (5): Wilhite et al. (2008). (6): Collier and Peterson (2001).

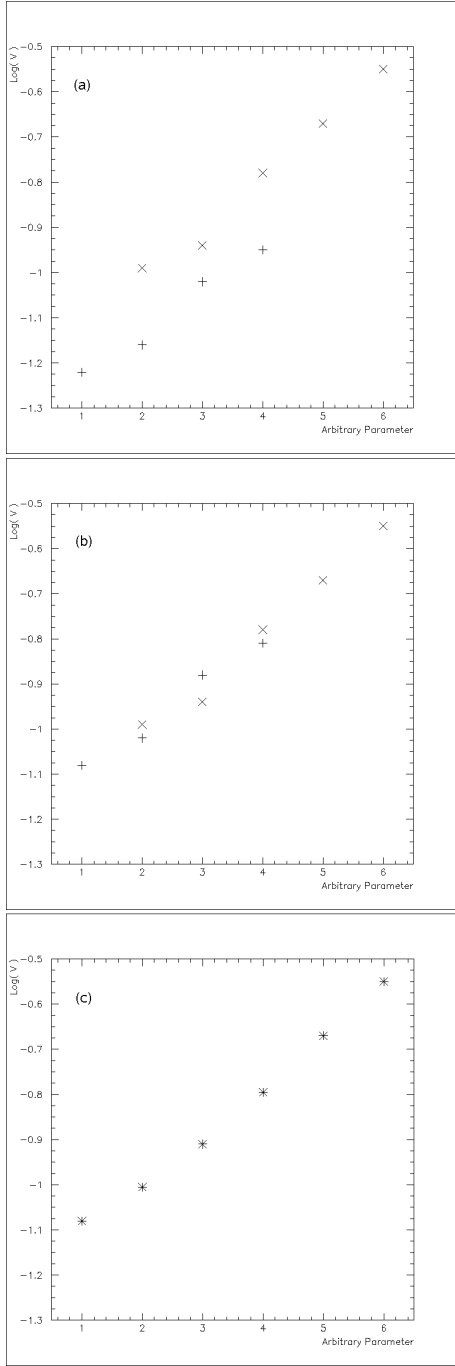


Fig. 4.— Illustration of the normalization procedure. \times and $+$ symbols represent two different data sets; the $+$ data are normalized to the \times set in panel (b), and averaged to yield the $*$ points in panel (c).

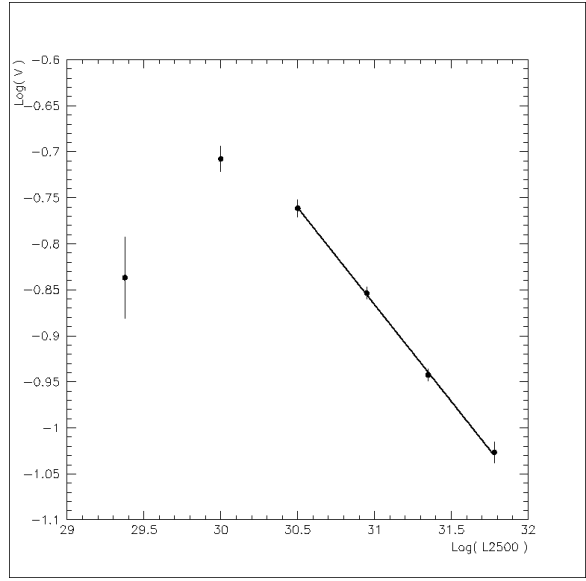


Fig. 5.— Logarithm of quasar variability V vs. logarithm of optical luminosity at 2500 \AA , with a linear fit of the brightest four points.

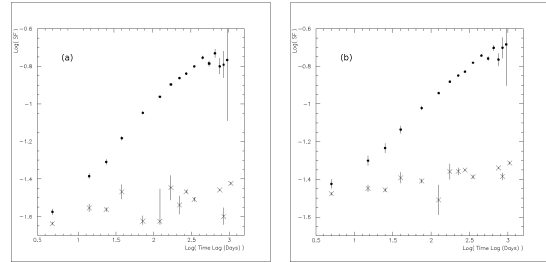


Fig. 6.— QUEST logarithmic structure functions vs. logarithmic rest frame time lag. (a): $SF^{(A)}$. (b): $SF^{(B)}$. Solid points: quasar results. \times : sample pointlike objects.

Model Type	SF Slope	Ref.
Microlensing	0.25 ± 0.03	(1)
Disk Instability	0.44 ± 0.03	(2)
Starburst	0.83 ± 0.08	(2)

Table 5: Comparison of theoretical quasar structure function slopes. Reference (1) indicates Hawkins (2002). (2): Kawaguchi et al. (1998).

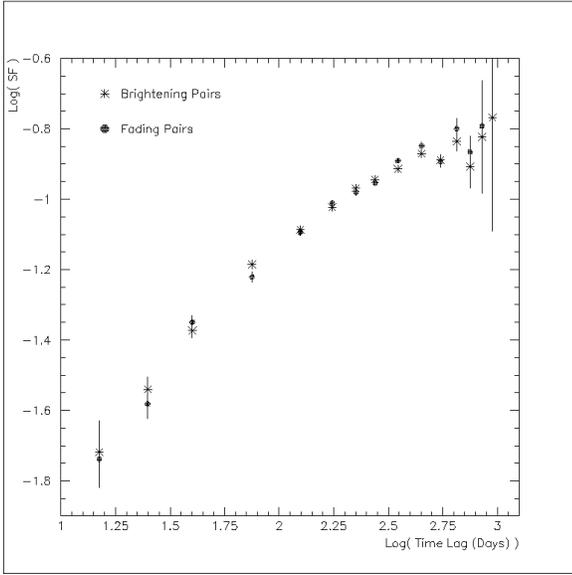


Fig. 7.— Logarithmic quasar structure function vs. logarithmic rest frame time lag using only brightening (asterisks) and fading (solid circles) magnitude pairs.

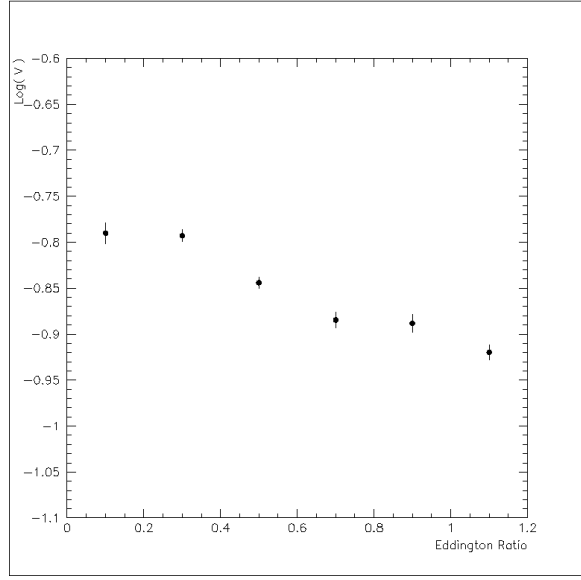


Fig. 9.— Logarithm of quasar variability V vs. Eddington ratio.

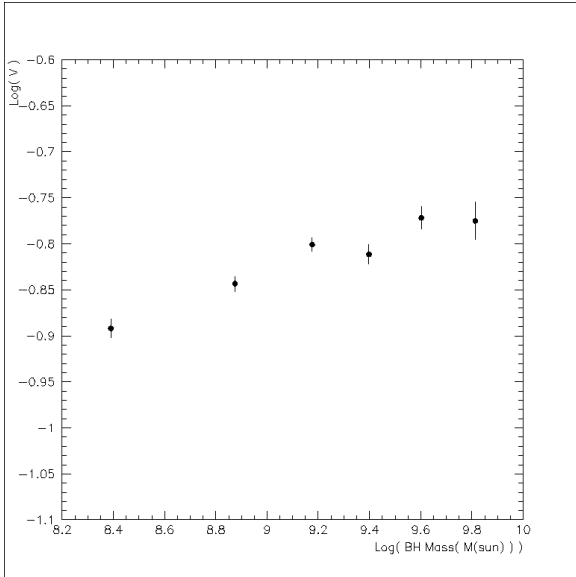


Fig. 8.— Logarithm of quasar variability V vs. estimated black hole mass.

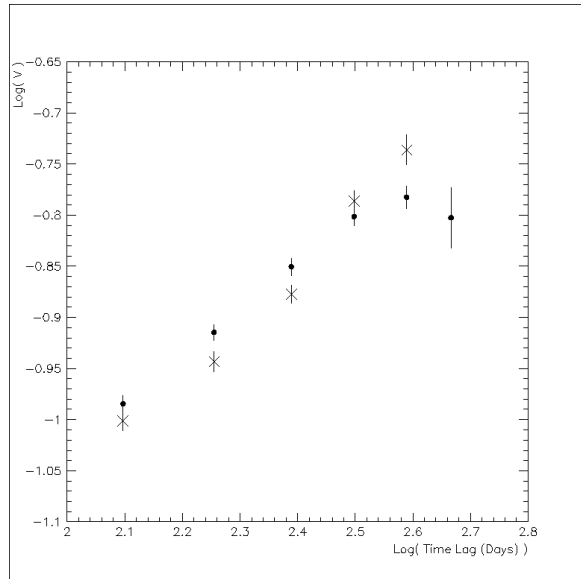


Fig. 10.— Logarithm of quasar variability vs. logarithm of rest frame time lag for only low Eddington ratio (solid circles) and high Eddington ratio (\times) objects.

however it illustrates the point that the relationship between variability amplitude and luminosity, and in particular the value of δ , does probe the physics of the system. Because V , defined in equation 6, is an approximation of Δm , equation 9 is equivalent to the relation

$$\log(V) = K - \delta \cdot \log(L) \quad (10)$$

where K is a constant.

We measure $\delta = 0.205 \pm 0.002$. Clearly our results are inconsistent with the most basic Poissonian prediction. Vanden Berk et al. (2004) calculated δ using SDSS data to be 0.246 ± 0.005 , which is inconsistent with our result at the level of 6σ . Like ours, however, it is much shallower than the simple Poissonian prediction.

7.3. Variability vs. Black Hole Mass

Wold et al. (2007) have noted a positive correlation between quasar variability amplitude and black hole mass, using about 100 SDSS quasars seen in QUEST1 data. Because they do not correct for correlations between quasar parameters, they note that their results with respect to mass may be confounded with trends with respect to time lag. We confirm that the correlation is real, using much better statistics and more data at high masses. The trend can be roughly described by the relation

$$\log(V) \propto \mu \times \log(Mass).$$

The best fit yields a reduced χ^2 of 2.5 for $\mu = 0.13 \pm 0.01$.

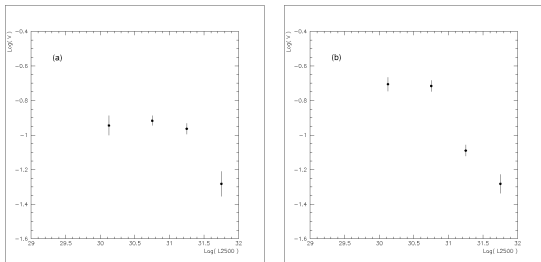


Fig. 11.— Logarithm of quasar variability V vs. logarithm of optical luminosity at 2500 \AA for objects with radio measurements. (a): objects with radio to optical ratio less than 20. (b): objects with ratios above 20.

Collier and Peterson (2001) notes a rough correlation between mass and characteristic variability timescale in their sample of 12 Seyfert 1 galaxies. We see no such correlation in the quasars' average behavior over the timescales studied here.

7.4. Variability vs. Eddington Ratio

The previously observed dependences of variability on luminosity and mass imply that variability amplitude should decrease with Eddington ratio. This fact was discussed by Wilhite et al. (2008), who measured the luminosity and mass relationships using repeated SDSS measurements of quasars in a 278 degree^2 equatorial strip and posited that the Eddington ratio may be the physically important parameter underlying both trends. While they noted that their highest Eddington ratio quasars were indeed the least variable, they did not explore the shape of the trend as has been done in this work, due to the fact that their sample included 10 times fewer quasars than studied here.

We see flat average variability at both low and high Eddington ratios, with a transition around a ratio of 0.5. The time dependence of variability also changes with the quasar's Eddington ratio, as shown in figure 10. Quasars with low Eddington ratio tend to vary more on shorter timescales than those with high Eddington ratio, which vary more on longer timescales. The behavior of the two groups is comparable around a rest frame time lag of 300 days. The variability mechanism therefore appears to change in quality between the two groups of objects, rather than simply quantity. This could be consistent with fluctuations from different physical processes for the two groups. Or, the Eddington ratio could reflect the same disk physics in each case, with lower Eddington ratios characteristic of disks with shorter variability timescales.

7.5. Variability vs. X-ray Emission

We see an anticorrelation between optical variability amplitude and X-ray luminosity at the level of 2.9σ . Our result is not inconsistent with the overall increase in variability from X-ray non-detections to detections seen by Vanden Berk et al. (2004) and Rengstorf et al. (2006); the average variability amplitude of all of our X-ray detected quasars is higher than that

of the remainder of the sample by more than 3σ . Rengstorf et al. (2006) note that the few nonvariable quasars in their X-ray detected sample have higher average X-ray flux than the variable X-ray detected quasars, and suggest an anticorrelation between X-ray luminosity and optical variability amplitude. Our results provide further evidence for such a relationship.

7.6. Variability vs. Radio Emission

There have been several reports of a positive correlation between optical variability amplitude and radio luminosity (e.g. Rengstorf et al. (2006)), although often the trend appears marginal (e.g. Vanden Berk et al. (2004)). Helfand et al. (2001) studied roughly 200 radio-selected quasars and saw that the optical variability amplitude was fairly constant across the range of radio loudness except for a possible increase for the radio loudest objects. We see no significant trend of optical variability amplitude with radio properties. The radio fainter and brighter subsets and the radio non-detections all have indistinguishable variability amplitudes. Furthermore, the anticorrelation between optical variability amplitude and optical luminosity is present for both radio louder and quieter samples. The similarities in optical variability, both in amplitude and versus optical luminosity, between the radio samples undermines the idea that different mechanisms may be responsible for the variability in radio quiet and radio loud quasars, as conjectured by Helfand et al. (2001).

7.7. Analogy with BHXBs

Black hole X-ray binaries, like quasars, are systems containing a central black hole and an accretion disk. BHXBs tend to be roughly 10^7 times less massive than quasars, and their accretion disk emission is correspondingly faster and of higher energy. X-ray observations of BHXBs over timescales of months can give insight into the behavior of quasars in optical and UV wavelengths over timescales that are too long to observe. BHXB behavior may therefore be uniquely helpful in the interpretation of quasar observations by allowing the quasar data to be considered in terms of a longer timescale framework.

In black hole X-ray binaries three states are observed. The low/hard state has Eddington ratios

of a few percent or less, low X-ray luminosity, a hard spectrum, and radio jets. It is thought to be dominated by emission from an energetic corona that is related to the accretion disk in a manner not well understood, and which is likely causally associated with the formation of radio jets. The high/soft state has stronger accretion, with Eddington ratios of a few percent or more, higher X-ray luminosity, a soft spectrum, and no radio jets. Its emission is hypothesized to be dominated by the accretion disk. The intermediate state has some elements of the former states' spectral properties, Eddington ratios of either a few percent or tens of percent, sometimes exhibits jets, and has more dramatic X-ray variability than either the low/hard or high/soft states. A thorough review of the X-ray variability of BHXBs can be found in van der Klis (2006).

The smaller scale of BHXBs means that both disk and coronal emission lie in X-ray bands. In quasar systems, the disk is further from the central engine and emits in the optical and UV range. The corona, however, still emits in X-ray wavelengths. Optical observations of quasars, then, may miss much of what corresponds to the low/hard X-ray state in BHXBs. Instead of observing disk-dominated emission and corona-dominated emission, we will observe primarily disk emission, but as modulated by other elements of the system.

We see a discrete shift in variability amplitude at intermediate Eddington ratio, implying that there may exist distinct phases in quasars that can be characterized by the Eddington ratio. Do our low and high Eddington ratio quasars have properties that are consistent with the X-ray binaries' states? Their average variabilities $\text{Log}(V)$, median X-ray loudnesses $\overline{\sigma_{ox}}$, and median radio loudnesses \overline{R} are given in table 6. The low Eddington ratio objects are on average more variable than the high Eddington ratio objects, as shown earlier. The median radio and X-ray properties are consistent between the two Eddington ratio groups. The time dependencies of the two groups' optical variability are slightly different, as shown in figure 10, with the lower Eddington ratio group varying more strongly at shorter timescales, and less strongly at longer timescales. These data best approximate the X-ray binary states if we compare our high Eddington sample with BHXBs in the high/soft state, and our low

Eddington sample with BHXBs in the intermediate state. This comparison matches the observed trends between Eddington ratio and average variability amplitude. The stronger accretion implied by higher Eddington ratios may be associated with a larger accretion disk, and therefore longer variability timescales; we indeed see longer variability timescales in the higher Eddington sample. The dampened variability amplitude in the larger disk may be due to discrete flares making a smaller fractional contribution to the flux. Or, the heightened variability amplitude in the lower Eddington state may be due to interactions with other parts of the system such as the corona.

Eddington ratio is not clearly correlated with radio loudness, as might be expected by an analogy with BHXBs. The high/soft BHXB state does not exhibit radio jets, while the intermediate state has occasional radio outflows. Since the intermediate state has on average more radio emission, the radio detections should be more variable on average than radio nondetections. The median radio loudness is indeed higher for the low Eddington ratio objects, as expected. However, the distributions have significant overlap, as shown by the large median deviations. A K-S comparison between the two sets of objects concludes that the radio loudnesses of the two groups has a probability $> 99.9\%$ of belonging to different underlying distributions. Therefore although we do not see a clearly defined trend, there is significant evidence that the two Eddington ratio groups have different radio properties. The low Eddington ratio subset is more radio loud than the high subset; this is the sense expected from an analogy with the intermediate and high/soft BHXB states.

We also see no clear-cut correlation between Eddington ratio and X-ray loudness α_{ox} . If our lower Eddington ratio sample had stronger coronal emission, as is the case in the BHXB intermediate state, we would expect to see stronger X-ray emission in this sample. The median α_{ox} of the two groups does show this trend, although two distributions have significant overlap. A K-S test between the two groups indicates that, despite the overlap, the α_{ox} of the two Eddington ratio subsets has $> 99.9\%$ probability of stemming from different underlying distributions. It has been noted by Vasudevan and Fabian (2007) that α_{ox} may be a poor indicator of AGN X-ray

to optical SED shape, as it stays roughly constant over a large range of observed spectral shapes. Indeed, Shemmer et al. (2008) see only a very weak correlation between Eddington ratio and α_{ox} in a sample of 35 radio-quiet AGN, while measuring a much stronger correlation between Eddington ratio and Γ , the hard X-ray spectral slope. This relationship between Eddington ratio and X-ray spectral hardness in quasars is of the same sense as the trend in BHXBs. Green et al. (2008) observe a shallow but significant correlation between Γ and α_{ox} in a sample of 1135 quasars; this trend, while subtle, is analagous to behavior in BHXB X-ray spectra in the high/soft state. A further link between AGN and BHXBs in X-ray observations is shown by Vasudevan and Fabian (2007), who determine that at Eddington ratios above 0.1 the X-ray emission from the corona is around four times weaker with respect to the total bolometric emission than in AGN with lower Eddington ratios. This information reinforces our optical evidence for quasar states modulated by the Eddington ratio, where high ratio objects show characteristics similar to the BHXB high/soft state, which is dominated by disk rather than coronal emission.

In summary, we see evidence for a distinct transition from a high accretion, larger disk scenario to one with stronger variability amplitude, shorter timescales, and less accretion. This behavior has parallels to the high/soft and intermediate states in BHXBs. We see some evidence for behavior from other parts of the system, such as a corona and jet, which may be associated with such a transition. The low and high Eddington ratio groups have significantly different radio and X-ray loudness properties. The radio and X-ray distributions for the two groups significantly overlap, however, complicating an interpretation of the data.

	$0 < E < 0.4$	$0.6 < E < 1$
$\text{Log}(V)$	-0.922 ± 0.005	-1.016 ± 0.006
$\overline{\alpha_{ox}}$	1.29 ± 0.09	1.37 ± 0.09
\overline{R}	28 ± 22	21 ± 17

Table 6: $\text{Log}(V)$, median X-ray loudness $\overline{\alpha_{ox}}$, and median radio loudness \overline{R} for quasars with low and high Eddington ratios E .

8. Conclusions

We have studied the ensemble optical variability of roughly 23,000 spectroscopically identified quasars using the Palomar-QUEST Survey. The survey's data were carefully cleaned and recalibrated for this variability work. The structure function was used to measure the quasar variability amplitude's dependence on time lag, and a power law exponent was fitted using several analysis methods. There is no evidence in our data for quasar lightcurve asymmetries. The variability amplitude was seen to decrease with increasing optical luminosity, a trend observed before although with a slightly different strength. Black hole mass is positively correlated with optical variability amplitude, with a steady increase seen over several orders of magnitude in mass. The relationships between variability amplitude and both luminosity and mass imply a decrease in variability amplitude with increasing Eddington ratio. We do see this trend; in particular we observe steady variability levels at low and high Eddington ratios, with a transition around Eddington ratio of 0.5. The increase in variability amplitude at low Eddington ratio is due to stronger fluctuations at timescales shorter than roughly 300 days; on timescales longer than 300 days the high Eddington ratio objects show stronger variability amplitude. X-ray data for about 850 of the quasars show an anticorrelation between optical variability amplitude and X-ray luminosity. Nearly 2,000 of the quasars have known radio fluxes; they show no dependence of optical variability amplitude on radio luminosity or detection. The discrete step nature of the optical variability amplitude vs. Eddington ratio results implies possible quasar states analogous to those in black hole X-ray binaries; our results indicate behavior similar to the binaries' intermediate state for low Eddington ratio quasars, and to the binaries' high/soft state for high Eddington ratio quasars.

We thank the Office of Science of the Department of Energy and the National Science Foundation for support.

Facilities: PO:1.2m

A. Modelling of the Structure Function

The Palomar-QUEST time sampling is finite and nonuniform. The structure function is therefore liable to include windowing effects due to the data cadence. To examine this effect we simulate quasar lightcurves which yield a power-law structure function when sampled uniformly. We then subject these lightcurves to our window function to study the effects of sampling.

A structure function of the form $SF^{(A)} \propto t^\beta$ is equivalent to a power spectral distribution (PSD) of the form $PSD \propto f^\alpha$, where $\alpha = -2\beta - 1$. Timmer and König (1995) present a method of computing light curves with power law spectra proportional to f^α through the careful choice of frequency amplitudes and phases. We use their method to simulate light curves, and confirm the expected relationship between the frequency dependence of the lightcurves and the structure function slope. An example evenly sampled, long timescale lightcurve and a structure function calculated from several such lightcurves are shown in figure 12. The lightcurve has a power spectral distribution $PSD \propto f^{-1.71}$, and the resulting structure function has logarithmic slope $\beta = 0.359 \pm 0.005$ which is consistent with the predicted value. The error bars in the plot are determined from the distribution of multiple instantiations of the simulation. The specific frequency dependence was chosen in order to approximately reproduce the slope of the experimental quasar structure function.

To study the effects of uneven data rates, we calculate the structure function from the simulated lightcurves using only data that align with our sampling cadence. In particular, for each quasar in the sample we generate a simulated lightcurve, centered at the average flux value measured for that quasar. We then replace each QUEST flux measurement with the value of the simulated lightcurve at the appropriate date, with added Gaussian noise on the order of our measurement errors. In this way the times of our measurements are unchanged between the real and simulated data, allowing us to study our window function exactly. The resulting simulated structure function is shown in figure 13. The error bars are determined by the spread between results from different subsets of the data, as in the analysis of the real data. The amplitude of the lightcurves is set in order to match the resulting structure function plot's y axis offset with the data. In order to approximate the real data, the maximum lightcurve variations over the 3.5 year timescale of the survey were set to be roughly one magnitude. Because the lightcurves have sharp peaks and our sampling is sparse, the true maxima were most often not observed. The first data point is affected by obvious edge effects due to the fact that the minimum time difference sampled in the simulated lightcurve is one day while the real data extends to shorter timescales. Note the flattening of the curve at high time lags where the window function is most influential. The turnover in the experimental quasar structure function should therefore be attributed to a windowing effect rather than evidence for a maximum timescale of variability.

The logarithmic slope of the linear region of the simulated, windowed structure function is measured to be $\beta = 0.341 \pm 0.029$, consistent with the value of 0.359 ± 0.005 shown in figure 12 which was calculated using lightcurves with close, even sampling and the same frequency dependence. The details of our data cadence therefore do not significantly affect the power law index of the structure function, given a power law frequency distribution of fluctuations.

The qualitative similarities in shape between our measured and simulated structure functions justifies the use of our chosen lightcurve model in examining the effects of uneven data sampling. The errors on the windowed, simulated structure function, however, are larger than those in the real data. This is because the spread in values of the structure function points is larger when using the simulated lightcurves. This difference implies that the simulated lightcurves may not accurately reflect the true statistical distribution of the variability. For the purposes of qualitatively understanding the effects of our data cadence, however, this parameterization is sufficient.

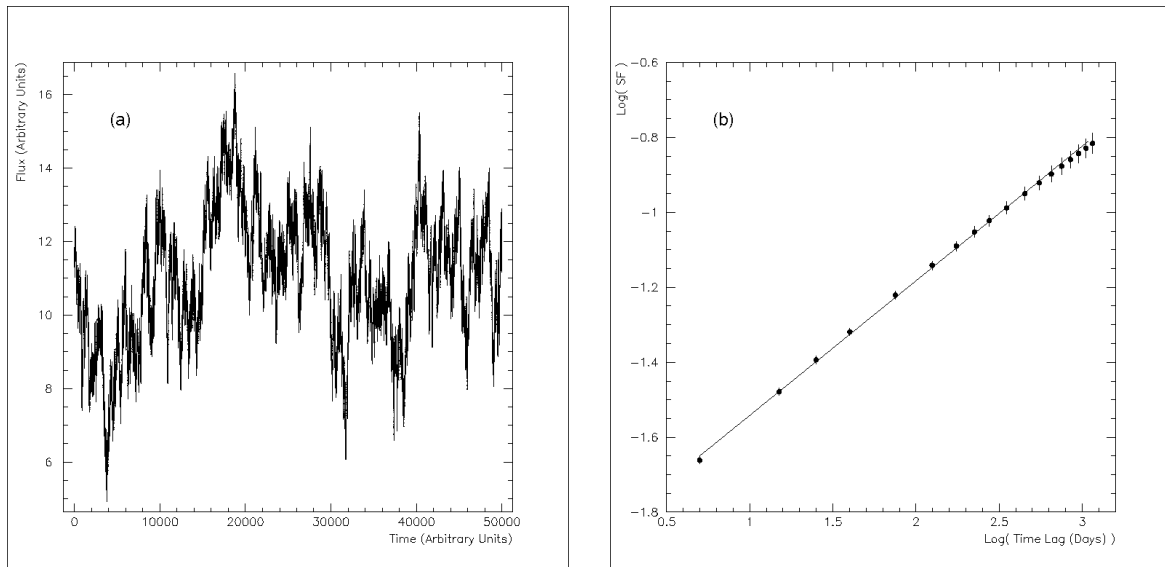


Fig. 12.— (a): A sample simulated lightcurve with $\alpha = -1.71$. (b): The structure function calculated from such simulations, with a fitted power law superimposed. Plotted on a log-log scale.

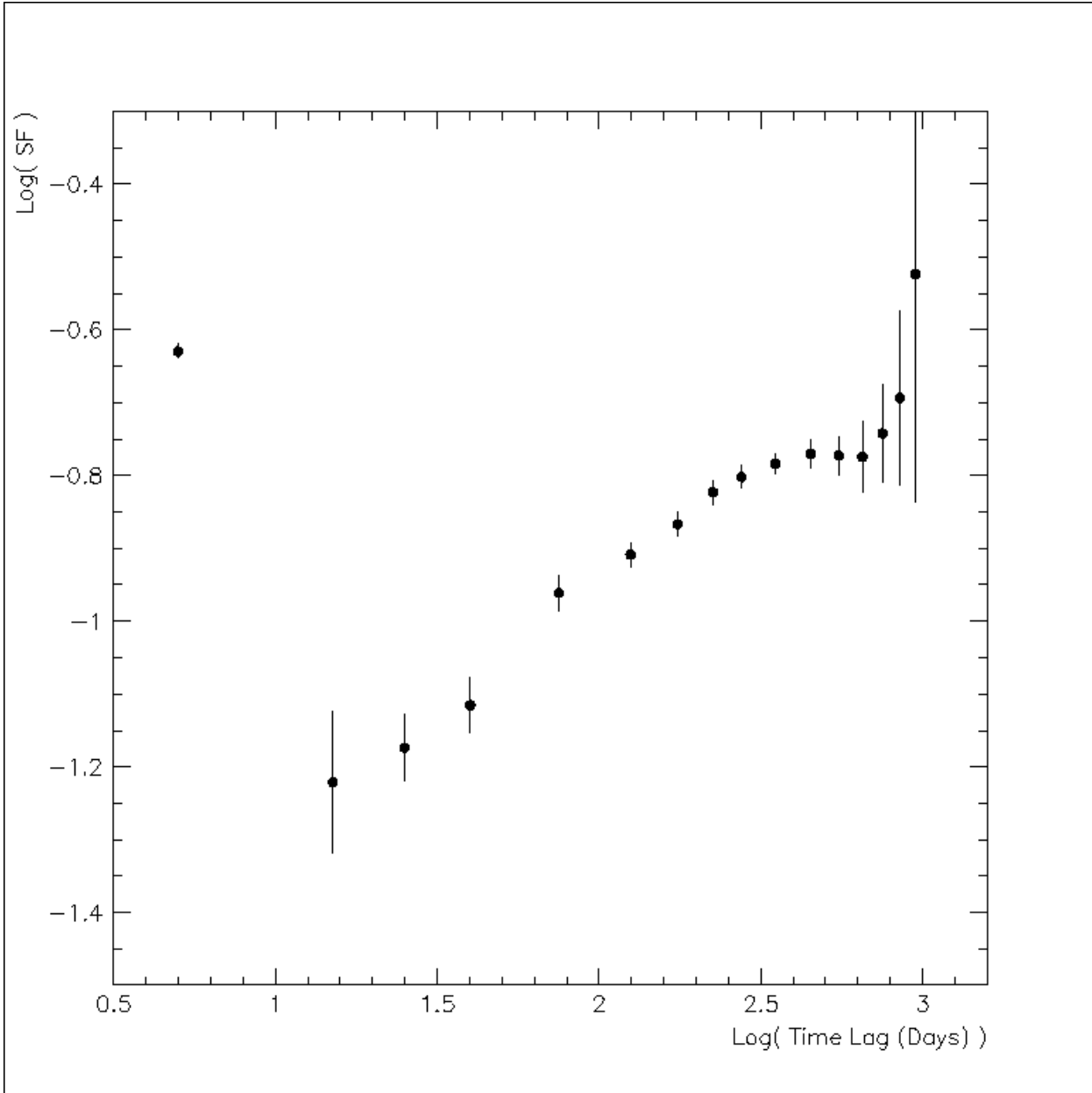


Fig. 13.— The structure function calculated from simulated lightcurves and passed through the QUEST window function, with a fitted power law superimposed. Plotted on a log-log scale.

REFERENCES

- Adelman-McCarthy, J. et al. 2006, *ApJS*, 162, 38
- Anderson, S. et al. 2007, *AJ*, 133, 313
- Andrews, P. et al. 2008, *PASP*, 120, 703
- Aretxaga, I. et al. 1997, *MNRAS*, 286, 271
- Baltay, C. et al. 2007, *PASP*, 120, 703
- Becker, R. et al. 1995, *ApJ*, 450, 559
- Cid Fernandes, R. et al. 2000, *ApJ*, 544, 123
- Collier, S. and Peterson, B. 2001, *ApJ*, 555, 775
- Collinge, M. et al. 2005, *AJ*, 129, 2542
- De Vries, W. et al. 2005, *AJ*, 129, 615
- Di Clemente, A. et al. 1996, *ApJ*, 463, 466
- Giommi, P. et al. 2002, in *Blazar Astrophysics with BeppoSAX and Other Observatories*
- Green, P.J. et al. 2008, *ApJS*, in press (arXiv:0809.1058)
- Hawkins, M. 2002, *MNRAS*, 329, 76
- Healey, S. et al. 2007, *ApJS*, in press (arXiv:0709.1735)
- Helfand, D. et al. 2001, *AJ*, 121, 1872
- Hewitt, A. and Burbidge, G. 1993, *ApJS*, 87, 451
- Huber, M.E. et al. 2006, *AJ*, 132, 633
- Kaspi, S. et al. 2000, *ApJ*, 533, 631
- Kawaguchi, T. et al. 1998, *ApJ*, 504, 671
- Massaro, E. et al. 2007, *AIP Conference Proceedings*, 921, 349
- Monet, D. et al. 1998, *Bulletin of the American Astronomical Society*, 38, 1427
- Pereyra, N.A. et al. 2006, *ApJ*, 642, 87
- Peterson, B.M. 1997, *An Introduction to Active Galactic Nuclei* (Cambridge University Press)
- Pickles, A. 1998, *PASP*, 110, 863
- Rengstorf, A. et al. 2006, *AJ*, 131, 1923
- Salviander, S. et al. 2007, *ApJ*, 662, 131
- Sesar, B. et al. 2006, *AJ*, 131, 2801
- Shemmer, O. et al. 2008, *ApJ*, 682, 81
- Shields, G. et al. 2003, *ApJ*, 583, 124
- Sowards-Emmerd, D. et al. 2005, *ApJ*, 626, 958
- Stickel, M. et al. 1991, *ApJ*, 374, 431S
- Timmer, J. and König, M. 1995, *A&A*, 300, 707
- Turriziani, S. et al. 2007, *A&A*, 472, 699
- van der Klis, M. 2006, in *Compact Stellar X-ray Sources* (Cambridge University Press), 39
- Vanden Berk, D. et al. 2001, *AJ*, 122, 549
- Vanden Berk, D. et al. 2004, *ApJ*, 601, 692
- Vasudevan, R. and Fabian, A. 2007, *MNRAS*, 381, 1235
- Veron-Cetty, M. and Veron, P. 2006, *A&A*, 455, 773
- Wilhite, B. et al. 2005, *ApJ*, 633, 638
- Wilhite, B. et al. 2008, *MNRAS*, 383, 1232
- Wold, M. et al. 2007, *MNRAS*, 375, 989
- Zackrisson, E. et al. 2003, *A&A*, 408, 17

This 2-column preprint was prepared with the AAS L^AT_EX macros v5.2.